Journal of proteome research

Article

pubs.acs.org/jpr

Quantitative Proteomic Analysis Reveals That Transmissible Gastroenteritis Virus Activates the JAK-STAT1 Signaling Pathway

Kang An,[†] Liurong Fang,*[,†] Rui Luo,[†] Dang Wang,[†] Lilan Xie,[‡] Jing Yang,[†] Huanchun Chen,[†] and Shaobo Xiao*[,†]

[†]Division of Animal Infectious Diseases, State Key Laboratory of Agricultural Microbiology, College of Veterinary Medicine, Huazhong Agricultural University, Wuhan, Hubei China

[‡]Department of Biotechnology, Wuhan Institute of Biological Engineering, Wuhan, Hubei China

Supporting Information

ABSTRACT: Transmissible gastroenteritis virus (TGEV), a porcine enteropathogenic coronavirus, causes lethal watery diarrhea and severe dehydration in piglets. In this study, liquid chromatography−tandem mass spectrometry coupled to isobaric tags for relative and absolute quantification labeling was used to quantitatively identify differentially expressed cellular proteins after TGEV infection in PK-15 cells. In total, 162 differentially expressed cellular proteins were identified, including 60 upregulated proteins and 102 downregulated proteins. These differentially expressed proteins were involved in the cell cycle, cellular growth and proliferation, the innate immune response, etc. Interestingly, many upregulated proteins were associated with interferon signaling, especially signal transducer and activator of transcription 1 (STAT1) and interferon-stimulated genes (ISGs). Immunoblotting and real-time quantitative reverse transcription polymerase chain reaction demonstrated that TGEV infection induces STAT1 phosphorylation and nuclear translocation, as well as ISG expression. This study for the first time reveals that TGEV induces interferon signaling from the point of proteomic analysis.

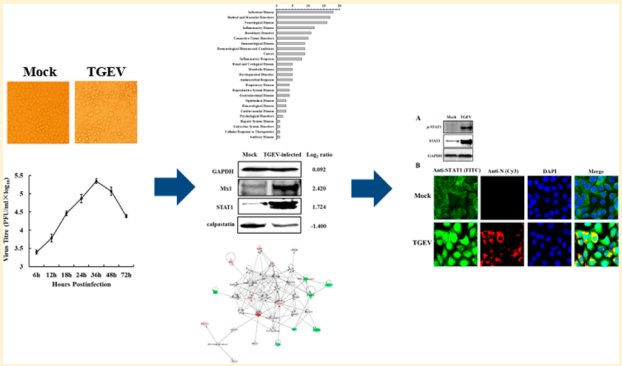

KEYWORDS: *transmissible gastroenteritis virus (TGEV), isobaric tags for relative and absolute quantitation (iTRAQ), proteomics, interferon signaling*

INTRODUCTION

Transmissible gastroenteritis is an acute enteric disease of swine, with clinical symptoms typified by lethal watery diarrhea and severe dehydration in piglets. Because mortality can be up to 100% in infected piglets less than 3 weeks old, this disease always causes high economic losses once outbreaks occur, and it is therefore an ongoing threat to the development of the swine industry.[1,2] The causative agent, transmissible gastroenteritis virus (TGEV), is a member of the family Coronaviridae in the order Nidovirales.[3] The genome of TGEV contains a single-stranded plus-sense RNA of approximately 28.5 kb in length.[4] At least nine open reading frames (ORFs) have been identified or predicted in the TGEV genome, and the two largest ORFs (ORF1a and ORF1b) in the 5′-proximal two-thirds of the genome encode the viral replicase.[5] The 3′ one-third of the genome encodes viral structural and accessory proteins, including the spike (S) glycoprotein, membrane (M) glycoprotein, nucleocapsid (N) protein, a small envelope (E) glycoprotein, and three accessory proteins 3a, 3b, and 7.[6] Multiple functions and activities have been identified for the structural and accessory proteins. For example, the large glycoprotein S, located on the virion's surface, binds the host cell receptor and mediates membrane fusion;[7] the M protein is largely embedded in the membrane and plays a crucial role in the assembly of the virion;[8,9] the E protein, a minor structural component, is essential for intracellular viral trafficking through the secretory pathway and full virus maturation,[10,11] but the three accessory proteins, 3a, 3b, and 7, are not essential for viral replication.[12,13] Despite years of intensive research into the characterization and function of the individual proteins encoded by TGEV, the mechanisms of TGEV pathogenesis and immunomodulation remain largely unclear.

During the past decade, proteomic methods have become important tools with which to study host cellular responses to viral infection and provide specific insights into the cellular mechanisms involved in viral pathogenesis. For example, Emmott et al. investigated the changes in the host cell proteome that occur in response to infectious bronchitis virus (IBV) using stable isotope labeling of amino acids in cell culture (SILAC) in conjunction with liquid chromatography−

Received: February 21, 2014
Published: October 30, 2014

dx.doi.org/10.1021/pr500173p | J. Proteome Res. 2014, 13, 5376−5390

tandem mass spectrometry (LC−MS/MS) and identified 1830 cellular and two viral proteins in IBV-infected cells.[14] Zhang et al. defined 158 host proteins involved in Japanese encephalitis virus infection with a SILAC-based quantitative proteomic analysis.[15] Jiang and co-workers analyzed the cellular response to severe acute respiratory syndrome-associated coronavirus (SARS-CoV) infection by combining two proteomic methods and identified 186 proteins differentially expressed in infected and mock-infected cells.[16] Coombs et al. used a SILAC technique, combined with high-throughput two-dimensional (2D) high-performance liquid chromatography (HPLC)−MS to identify 280 differentially expressed proteins in host cells infected with human influenza virus.[17] Fan et al. used SILAC coupled to MS to identify 163 proteins with significantly altered expression in porcine circovirus type 2 (PCV2)-infected cells compared with uninfected cells.[18] These studies have not only increased our understanding of the host response to viral infection but also highlighted potential targets for the development of antiviral agents.

Isobaric tags for relative and absolute quantification (iTRAQ) combined with LC−MS/MS analysis has emerged as a powerful quantitative proteomic method because it has several remarkable advantages over traditional proteomic approaches, including its high-throughput, high sensitivity, and greater accuracy. The iTRAQ-based quantitative proteomic technique has been used in studies of virus−host interactions for several important viruses, including human immunodeficiency virus (HIV-1),[19] hepatitis B virus,[20] Epstein−Barr virus,[21] porcine reproductive and respiratory syndrome virus (PRRSV),[22] and PCV2.[23] In this study, we quantitatively identified the cellular proteins differentially expressed after TGEV infection of PK-15 cells using an iTRAQ-based proteomic approach. At 24 h after TGEV infection, the expression of 162 proteins was significantly altered. A bioinformatic analysis revealed that these differentially expressed cellular proteins were assignable to several biological systems and processes. Most importantly, we found that many upregulated proteins were associated with interferon signaling. Further detailed experiments demonstrated that TGEV infection activates the janus kinase signal transducer and activator of the transcription 1 (JAK-STAT1) signaling pathway.

EXPERIMENTAL SECTION

Virus and Cells

Porcine kidney (PK-15) cells were purchased from the China Center for Type Culture Collection (CCTCC, Wuhan, China) and grown in Dulbecco's modified Eagle's medium (Invitrogen, Carlsbad, CA, USA), supplemented with 10% fetal bovine serum (Invitrogen) at 37 °C under 5% CO_2. TGEV strain WH-1 (GenBank accession no. HQ462571), which was isolated in China, was propagated in PK-15 cells, and the viral titer was determined by plaque assay.

Virus Inoculation

Confluent PK-15 cells in 10 cm^2 cell culture dishes were inoculated with TGEV strain WH-1 at a multiplicity of infection (MOI) of 0.1. Uninfected cells were used as the mock-infected group. The cells were collected for protein isolation, digestion, and labeling 24 h postinfection (hpi). Viral propagation was confirmed by observation of the cytopathic effect (CPE) and the one-step growth curve of TGEV strain WH-1 in PK-15 cells.

Protein Isolation, Digestion, and Labeling with iTRAQ Reagents

The TGEV-infected group and controls, including three independent biological replicates, were collected with a cell scraper, centrifuged at 300*g* for 10 min, and washed twice with ice-cold phosphate-buffered saline (PBS) containing 1 mM pervanadate and 1 mM sodium fluoride. The collected cells were lysed in 500 μL of lysis buffer containing 1 mM PMSF, 2 mM EDTA, and 10 mM DTT, and the soluble protein fraction was harvested by centrifugation at 25 000*g* for 20 min at 4 °C. The protein concentration of the supernatant was determined with the Bradford method with BSA as the standard.[24] Solutions containing precisely 100 μg of protein were digested for 8 h at 37 °C with sequencing-grade modified trypsin and then labeled with different iTRAQ tags as follows: the three mock-infected samples were each labeled with iTRAQ 113 (IT113), iTRAQ 114 (IT114), or iTRAQ 115 (IT115); and the three TGEV-infected samples were each labeled with iTRAQ 116 (IT116), iTRAQ 117 (IT117), or iTRAQ 118 (IT118). The labeled samples were then mixed and dried with a rotary vacuum concentrator.

LC−MS/MS Analysis

After separation by strong cation exchange chromatography on a 20AB HPLC system (Shimadzu, Kyoto, Japan), the labeled peptide mixtures were eluted with 4 mL of buffer A (25 mM NaH_2PO_4 in 25% acetonitrile [ACN], pH 2.7) for 10 min at a flow rate of 1 mL/min, and then gradually mixed with 5−35 and 35−80% buffer B (25 mM NaH_2PO_4, 1 M KCl in 25% ACN, pH 2.7) for 11 and 1 min, respectively. The whole elution process was monitored by the absorbance at 214 nm. A total of 20 fractions were collected with screening. Each fraction was desalted with a StrataX desalting column and lyophilized. Equal amounts of digested protein in a final volume of 9 μL were introduced into a Symmetry C18 trapping column (5 μm particles, 180 μm inner diameter × 20 mm; Waters) with the nanoACQUITY Sample Manager (Waters) and washed with solvent A (98% H_2O, 2% acetonitrile, and 0.1% formic acid) for 15 min at 2 μL/min. Using solvent A and solvent B (98% acetonitrile, 2% H_2O, and 0.1% formic acid), the peptides were eluted from the trapping column over a BEH 130 C18 column (1.7 μm particles, 100 μm inner diameter × 100 mm) with a gradient (5% B for 1 min at 300 nL/min, 5−35% B for 40 min, 35−80% B for 5 min, and 80% B for 5 min) using a nanoACQUITY UPLC system (Waters). MS/MS was performed with a Triple TOF 5600 mass spectrometer (AB Sciex, Concord, ON). The ion source was a NanoSpray III source (AB Sciex) and the radiator was a needle made of quartz material (New Objectives, Woburn, MA). During data acquisition, the machine parameters were set to the parallel fragmentation mode with scan times of 3.3 s, and the fragmentation energy was set to 35 ± 5 eV.

Data Analysis

The acquired MS raw data files were converted into MGF files using 5600 msconverter, and the MGF files were searched. MS/MS data were searched against the pig subset database from the NCBInr database (release April 2013, containing 42 698 sequences), and the proteins were identified by using Mascot search engine (Matrix Science, London, UK; version 2.3.02). For protein identification, a mass tolerance of 0.05 Da was permitted for intact peptide masses and 0.1 Da for fragmented ions, with allowance for one missed cleavage in the trypsin digests: Gln → pyro-Glu (N-term Q), oxidation (M),

dx.doi.org/10.1021/pr500173p | J. Proteome Res. 2014, 13, 5376−5390

deamidated (NQ) as the potential variable modifications, and carbamidomethyl (C), iTRAQ8plex (N-term), and iTRAQ8-plex (K) as fixed modifications. The charge states of peptides were set to +2 and +3. Specifically, an automatic decoy database search was performed in Mascot by choosing the decoy checkbox in which a random sequence of database was generated and tested for raw spectra as well as the real database. To reduce the probability of false peptide identification, only peptides with significance scores greater than "identity_score" were counted as identified, and each confident protein identification involves at least one unique peptide. The quantitative protein ratios were weighed and normalized by the median ratio in Mascot. For comparison between samples, $\log_2$ ratio of $\geq$0.585 or $\leq$−0.585 (fold change $\geq$1.5 or $\leq$0.667) and a p value <0.05 were considered as significantly different expressions according to the t-test. To better visualize the annotated tandem mass spectra, Mascot data files were loaded into Scaffold Q+ 4.3.4 software. The software was only used to visualize and export the spectra, with no normalization or data filtration were taken.

Immunofluorescence Assay

PK-15 cells were seeded on cover glasses (NEST Biotechnology) in 24-well plates until the cells reached approximately 70−80% confluence, and then the cells were infected with TGEV (MOI 0.1) and fixed with cold 4% paraformaldehyde at 24 hpi. The TGEV-infected cells were detected with mouse monoclonal antibody directed against the TGEV N protein (made in our laboratory) and Cy3-labeled goat anti-mouse IgG antibody (Sigma). The endogenous STAT1 was detected by rabbit polyclonal antibody directed against STAT1 (Cell Signaling Technology, Inc.) and FITC-labeled goat anti-rabbit IgG (Sigma). Cell nuclei were counterstained with 0.01% 4′,6-diamidino-2-phenylindole (DAPI; Invitrogen). The fluorescent images were examined under a confocal laser scanning microscope (LSM 510 Meta, Carl Zeiss).

RNA Extraction and Real-Time RT-PCR

Total cellular RNA was extracted with TRIzol reagent (Invitrogen) from TGEV-infected PK-15 cells. After the RNA (0.4 μg) was reverse-transcribed to cDNA, real-time reverse transcription polymerase chain reaction (RT-PCR) assays were performed with an Applied Biosystems ViiA 7 real-time RT-PCR system in a 10 μL volume containing 50 ng of the cDNA template, FastStart DNA Master SYBR Green I Mix reagent kit (Roche), and 100 nM of each primer. The pairs of gene-specific primers used for real-time RT-PCR are shown in Supplementary Table 1. Each cDNA sample was amplified in triplicate. The thermal cycling conditions were 10 min at 95 °C and 40 cycles of 10 s at 95 °C, 20 s at 56 °C, and 30 s at 72 °C. Gene expression was measured with a relative quantitative analysis of the data using the Applied Biosystems ViiA 7 real-time RT-PCR system software in a relative quantification (ΔΔCt) model (Applied Biosystems).

Immunoblotting Analysis

The protein concentrations in the TGEV-infected and mock-infected cell lysates, harvested at 24 hpi, were measured. Equivalent amounts of cell lysates from the three independent biological replicates were denatured in 5× sample loading buffer by heating at 95 °C for 10 min and were then separated by 10% SDS-PAGE. The proteins were electrotransferred to 0.45 μm PVDF membranes (Millipore). The membranes were blocked with 5% nonfat dry milk in Tris-buffered saline (TBS) containing 0.05% Tween 20 (TBST) for 2 h at room temperature and then incubated overnight at 4 °C with mouse polyclonal antibody directed against GAPDH (Boster, China), rabbit polyclonal antibody directed against STAT1 (Cell Signaling Technology, Inc.), rabbit polyclonal antibody directed against phospho-STAT1 (Tyr701; Cell Signaling Technology, Inc.), rabbit polyclonal antibody directed against Mx1 (Protein-Tech, Wuhan, China), or rabbit polyclonal antibody directed against calpastatin (Protein-Tech). The membranes were washed with TBST and incubated with horseradish peroxidase (HRP)-conjugated goat anti-mouse IgG antibody (Beyotime, China) or HRP-conjugated goat anti-rabbit IgG antibody (Beyotime) for 2 h. After the membranes were washed three times with TBST, the signals were developed using the Clarity Enhanced Chemiluminescence (ECL) reagent (Bio-Rad, Hercules, CA).

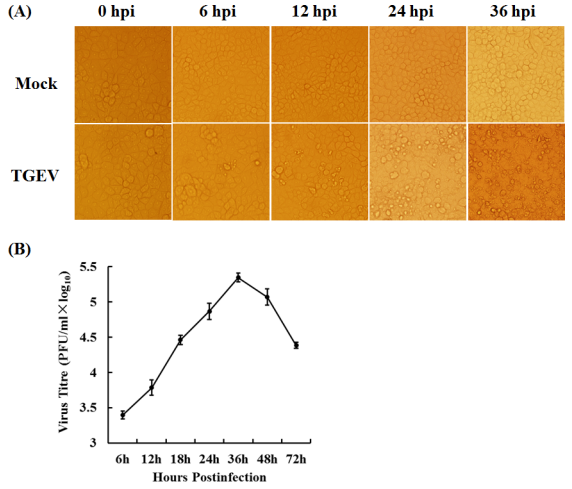

Figure 1. Virus infection. (A) Photomicrographs of PK-15 cells infected with TGEV strain WH-1 at MOI = 0.1 or mock-infected at different times after infection (indicated at top). Images were taken at an original magnification of 40×. (B) One-step growth curve of TGEV strain WH-1 in PK-15 cells.

RESULTS

Identification of 162 Differentially Expressed Cellular Proteins in TGEV-Infected PK-15 Cells

To identify an optimal time point after TGEV infection for the proteomic analysis, PK-15 cells were infected with TGEV strain WH-1 at an MOI of 0.1 and microscopically monitored for CPE at 0, 6, 12, 24, and 36 hpi. As shown in Figure 1A, the minimal CPE became visible at 12 hpi, and the CPE was readily apparent as the infection progressed. Up to 36 hpi, the infected cells deceased rapidly and an obvious CPE was observed. The one-step growth curve for TGEV strain WH-1 in PK-15 cells was assessed. As shown in Figure 1B, the viral titer reached a plateau of approximately 5.3 $\log_{10}$ at 36 hpi and then gradually and continuously declined. Generally, the time point at which viral replication remains high but no significant host cell cytoskeleton or membrane rearrangement is observed is the optimal time for a proteomic analysis.[15] Based on the CPE and titer analyses, we chose 24 hpi as the time point under our infection conditions for further proteomic analysis.

The collected TGEV-infected and mock-infected PK-15 cells were treated as described in the Experimental Section for iTRAQ-coupled LC−MS/MS analysis. A total of 10 053 peptides and 3062 proteins were detected and quantified by

dx.doi.org/10.1021/pr500173p | J. Proteome Res. 2014, 13, 5376−5390

Table 1. Statistically Significant Differentially Expressed Proteins Identified by iTRAQ Analysis of PK-15 Cells Infected with TGEV[a]

protein name	accession no.	$\log_2$ ratios (infection/control)	peptides	sequence coverage (%)	functions
proteins present in increased abundance in TGEV-infected cells					
ISG15 ubiquitin-like modifier	gil 187373263	3.84	4	25.9	type I interferon-mediated signaling pathway
interferon-induced protein with tetratricopeptide repeats 3	gil 324123893	2.97	5	18.5	type I interferon-mediated signaling pathway
interferon-induced protein with tetratricopeptide repeats 2	gil 395147196	2.65	4	10	type I interferon-mediated signaling pathway
interferon-induced protein with tetratricopeptide repeats 1	gil 346986269	2.57	4	10.1	type I interferon-mediated signaling pathway
Mx1	gil 156720190	2.42	9	16.8	type I interferon-mediated signaling pathway
60S ribosomal protein L31-like	gil 335308216	2.10	1	11.2	structural constituent of ribosome
histone H2A type 1-F-like	gil 335291882	2.09	2	21.5	nucleosome assembly
Mx2 protein	gil 210050415	2.04	12	21.9	type I interferon-mediated signaling pathway
2′-5′ oligoadenylate synthetase	gil3451331	1.81	3	9.7	type I interferon-mediated signaling pathway
2′-5′ oligoadenylate synthetase 2	gil45594389	1.79	7	16.4	type I interferon-mediated signaling pathway
signal transducer and activator of transcription 1 transcript variant 1 (STAT1)	gil 353468889	1.72	6	10.4	signal transducer and transcription activator
hypothetical protein LOC100511612	gil 311276597	1.69	1	2	transcriptional regulator
probable arginyl-tRNA synthetase, mitochondrial-like	gil 335279221	1.39	2	5.2	arginine-tRNA ligase activity
RING finger protein 213-like, partial	gil 350590115	1.30	10	3.3	E3 ubiquitin-protein ligase
dolichyl-diphosphooligosaccharide-protein glycosyltransferase 48 kDa subunit	gil 218511750	1.22	6	16.2	dolichyl-diphosphooligosaccharide-protein glycotransferase activity
RAB10, member RAS oncogene family	gil 340007402	1.22	3	16.5	small GTPase-mediated signal transduction
ribosomal protein S10	gil 346421343	1.15	3	23	structural constituent of ribosome
nucleoporin-like 1 tv2	gil 456754131	1.04	2	4.6	component of the nuclear pore complex
40S ribosomal protein S3a, partial	gil45269041	1.04	5	22	structural constituent of ribosome
3-ketoacyl-CoA thiolase A, peroxisomal isoform 1	gil 311268663	1.04	2	8.5	palmitoyl-CoA oxidase activity
prenylcysteine oxidase-like	gil 335285324	1.03	1	2.1	prenylcysteine oxidase activity
mannosyl-oligosaccharide glucosidase	gil 311252326	1.03	2	3.9	mannosyl-oligosaccharide glucosidase activity
E3 ubiquitin-protein ligase UBR4	gil 350585700	0.98	4	2.1	ubiquitin-protein ligase activity
mRNA turnover 4 homologue	gil 343962640	0.97	3	12	mRNA turnover and ribosome assembly
integrin alpha-3-like	gil 350590446	0.97	6	8.2	integrin-mediated signaling pathway
39S ribosomal protein L10, mitochondrial-like	gil 311267458	0.96	2	13.7	structural constituent of ribosome
polymerase delta-interacting protein 3-like	gil 350583738	0.88	2	8.9	positive regulation of translation
60S ribosomal protein L27a-like isoform 1	gil 335294212	0.84	3	22.3	structural constituent of ribosome
tRNA pseudouridine synthase A, mitochondrial isoform 2	gil 194043580	0.82	4	10.4	pseudouridylate synthase activity
NAD-dependent malic enzyme, mitochondrial	gil 350578484	0.82	4	9.5	malate metabolic process
surfeit locus protein 4-like, partial	gil 335310428	0.80	2	14.1	Golgi organization
ATP-binding cassette, subfamily F (GCN20), member 2	gil 417515525	0.80	2	4.7	ATP catabolic process
60S ribosomal protein L7-like 1	gil 178057141	0.79	2	10.5	structural constituent of ribosome

dx.doi.org/10.1021/pr500173p | J. Proteome Res. 2014, 13, 5376−5390

Table 1. continued

protein name	accession no.	$\log_2$ ratios (infection/control)	peptides	sequence coverage (%)	functions
trans-2,3-enoyl-CoA reductase-like	gil 350580442	0.79	3	9.6	trans-2-enoyl-CoA reductase (NADPH) activity
polyribonucleotide nucleotidyltransferase 1	gil 336092205	0.76	5	7.4	positive regulation of mitochondrial RNA catabolic process
endoplasmic reticulum aminopeptidase 1	gil 417515570	0.75	6	7.9	aminopeptidase activity
calcium uniporter protein, mitochondrial	gil 194042794	0.74	6	28	calcium channel activity
mitochondrial NDUFA4	gil 117660613	0.73	1	14.6	cytochrome-c oxidase activity
lectin galactoside-binding soluble 9 protein	gil 213990518	0.72	5	16.3	carbohydrate binding
RPL23	gil 117661026	0.72	2	16.4	structural constituent of ribosome
rRNA 2′-*O*-methyltransferase fibrillarin-like isoform 1	gil 350585199	0.72	4	14.2	methyltransferase activity
bifunctional ATP-dependent dihydroxyacetone kinase/FAD-AMP lyase (cyclizing)	gil 403399477	0.70	5	14.3	glycerol metabolic process
guanine nucleotide-binding protein-like 3	gil 194041237	0.69	7	16.2	GTP binding
coatomer subunit gamma-2	gil 350539577	0.69	3	4.8	structural molecule activity
transferrin receptor protein	gil 298162731	0.68	7	9.1	peptidase activity
polymerase delta-interacting protein 2	gil 350590664	0.68	3	9.7	mitochondrion morphogenesis
ribosome biogenesis protein BRX1 homologue	gil 348605720	0.67	4	13.6	ribosome biogenesis
histone deacetylase complex subunit SAP18-like	gil 335296705	0.67	2	22.9	component of the SIN3-repressing complex
armadillo repeat containing 10	gil 349732194	0.67	3	16	regulation of growth
60S ribosomal protein L10	gil85681889	0.66	2	11.2	structural constituent of ribosome
WD repeat-containing protein 36-like	gil 350580979	0.65	8	10.6	T-cell activation and highly coregulated with IL2
NADH dehydrogenase [ubiquinone] iron-sulfur protein 8, mitochondrial-like isoform 2	gil 311247108	0.65	1	7.5	NADH dehydrogenase (ubiquinone) activity
ras-related protein R-Ras-like	gil 335290008	0.65	2	12.8	Ras protein signal transduction
mitochondrial import inner membrane translocase subunit Tim13-like	gil 335282345	0.60	3	36.8	zinc ion binding
cytosolic acyl coenzyme A thioester hydrolase	gil 350585538	0.60	2	6.6	fatty acid catabolic process
squalene epoxidase	gil 154089694	0.60	3	7.8	sterol biosynthesis
translocon-associated protein subunit delta-like isoform 1	gil 311277187	0.59	2	14	calcium ion binding
transmembrane emp24 domain-containing protein 2-like isoform 1	gil 335301140	0.59	3	18.9	vesicular protein trafficking
prohibitin 2	gil 343780941	0.59	10	40.1	negative regulation of estrogen receptor signaling pathway
NADH dehydrogenase [ubiquinone] 1 alpha subcomplex subunit 8	gil 298104126	0.59	2	14	NADH dehydrogenase (ubiquinone) activity
proteins present in decreased abundance in TGEV-infected cells					
CHORD containing protein-1	gil 162946616	−0.59	2	12	response to stress
clathrin light chain (CLTA) protein	gil 194595733	−0.59	2	18	structural molecule activity
FUS	gil 351738724	−0.59	4	8.3	RNA splicing
Radixin	gil131821	−0.59	10	20.2	actin filament capping
fibronectin isoform 2	gil 311273021	−0.60	21	12.8	peptidase activator activity
myb-binding protein 1A	gil 311268173	−0.60	27	25.6	regulation of transcription
U3 small nucleolar RNA-interacting protein 2-like	gil 335299134	−0.60	5	13.2	rRNA processing

dx.doi.org/10.1021/pr500173p | *J. Proteome Res.* 2014, 13, 5376−5390

Table 1. continued

protein name	accession no.	log_2 ratios (infection/control)	peptides	sequence coverage (%)	functions
proteins present in decreased abundance in TGEV-infected cells					
chromobox protein homologue 3-like isoform 2	gil 350595424	−0.61	5	29	regulation of transcription
putative rRNA methyltransferase 3	gil 311266963	−0.61	10	19.9	methyltransferase activity
LIM and SH3 protein 1	gil 456752935	−0.61	2	10	regulation of dynamic actin-based, cytoskeletal activities
microtubule-associated protein 4-like	gil 335299026	−0.61	15	20	microtubule assembly
proteasome subunit beta type-1	gil 346986249	−0.62	5	27.4	threonine-type endopeptidase activity
cell cycle exit and neuronal differentiation protein 1	gil8134343	−0.62	1	9.3	neuroblastoma cell differentiation
zinc finger protein ubi-d4	gil 311247329	−0.62	2	7.7	apoptotic signaling pathway
serine/threonine-protein kinase OSR1	gil73621342	−0.62	2	6.4	serine/threonine-protein kinase
double-strand-break repair protein rad21 homologue	gil 350582950	−0.63	3	7	apoptotic process
erythrocyte membrane protein band 4.1-like 2	gil 335279037	−0.63	9	14	structural molecule activity
pleckstrin homology-like domain, family B, member 2, partial	gil 335307977	−0.63	4	12.4	assembly of the postsynaptic apparatus
periaxin	gil 350585205	−0.64	36	38.5	nervous system development
guanine nucleotide-binding protein gamma 12 subunit	gil 166915512	−0.64	2	41.7	G-protein-coupled receptor signaling pathway
elongation factor 1-delta-like isoform 1	gil 350582854	−0.64	9	19.8	translation elongation factor activity
filamin-A-like, partial	gil 335310912	−0.64	7	41.2	actin binding
structural maintenance of chromosomes protein 4	gil 194041163	−0.64	5	4	cell cycle control, cell division, chromosome partitioning
myosin-14-like	gil 350585373	−0.65	20	24.1	regulation of cell shape
epidermal growth factor receptor kinase substrate 8-like protein 2-like	gil 311247012	−0.65	11	20.5	actin filament binding
activated RNA polymerase II transcriptional coactivator p15-like	gil 311272155	−0.65	2	17.9	regulation of transcription
14-3-3 protein eta	gil 194043292	−0.66	6	31.7	signal transduction
zinc finger matrin-type protein 2-like isoform 2	gil 350581181	−0.67	1	3.5	zinc ion binding
hypothetical protein LOC100623615	gil 350596569	−0.67	1	3.9	lymphocyte differentiation
la-related protein 1B-like	gil 350587811	−0.67	4	8.2	regulation of macroautophagy
tropomyosin alpha-1 chain	gil 148222268	−0.67	7	23.9	structural constituent of cytoskeleton
prostaglandin F2 receptor negative regulator	gil 350583487	−0.67	3	4.2	lipid particle organization
SEC16-like A	gil 456754346	−0.67	3	2.2	endoplasmic reticulum organization
LOW QUALITY PROTEIN: eukaryotic translation initiation factor 5B	gil 350582111	−0.68	7	8.9	regulation of translational initiation
elongation factor 1-beta	gil 343488474	−0.68	8	46.2	translation elongation factor activity
basal cell adhesion molecule-like	gil 350585312	−0.68	8	17.5	laminin receptor activity
coiled-coil−helix-coiled-coil−helix domain-containing protein 3, mitochondrial	gil 346644866	−0.68	1	4.8	regulation of transcription
14-3-3 protein theta isoform 1	gil 350582722	−0.69	9	44.1	signal transduction
unnamed protein product	gil1900	−0.69	4	17.8	sodium:potassium-exchanging ATPase activity
proteasome subunit alpha type-5	gil 222136590	−0.69	9	53.9	threonine-type endopeptidase activity
tumor protein D52	gil 346986324	−0.70	4	29.9	protein homodimerization activity/protein heterodimerization activity

dx.doi.org/10.1021/pr500173p | J. Proteome Res. 2014, 13, 5376−5390

Table 1. continued

protein name	accession no.	log_2 ratios (infection/control)	peptides	sequence coverage (%)	functions
proteins present in decreased abundance in TGEV-infected cells					
shootin-1-like isoform 1	gil 194042094	−0.70	5	9.7	membrane depolarization
chromodomain-helicase-DNA-binding protein 4	gil 417515864	−0.70	8	5.7	component of the histone deacetylase NuRD complex
filamin-B	gil 350591288	−0.70	10	24.3	actin binding
hypothetical protein LOC100522278	gil 350591535	−0.70	2	11.5	cell proliferation
CD44 antigen-like	gil 350580163	−0.71	3	10.4	receptor for hyaluronic acid (HA)
ran-specific GTPase-activating protein	gil 297307137	−0.71	3	18.4	GTPase activator activity
LOW QUALITY PROTEIN: dynactin subunit 1	gil 350582222	−0.71	10	11.2	transport
uncharacterized protein C19orf43-like	gil 311248909	−0.71	1	14.6	unknown
182 kDa tankyrase-1-binding protein	gil 335281873	−0.71	15	15.3	protein binding
peroxisomal membrane protein PEX14 isoform 1	gil 311258435	−0.73	1	2.9	transcription corepressor activity/ microtubule binding
hypothetical protein LOC100624388	gil 335309724	−0.73	1	11.5	positive regulation of transcription
hsc70-interacting protein-like isoform 1	gil 350583750	−0.73	5	15.2	protein binding
src substrate cortactin-like	gil 350579849	−0.74	3	7.5	organization of the actin cytoskeleton and cell structure
nucleolin-like	gil 335309939	−0.75	16	30	the major nucleolar protein of growing eukaryotic cells
inverted formin-2-like	gil 335310921	−0.75	2	3.8	actin cytoskeleton organization
laminin subunit beta-1	gil 335295652	−0.75	7	6.5	extracellular matrix structural constituent
occludin	gil 239934655	−0.76	4	11.1	structural molecule activity
Na(+)/H(+) exchange regulatory cofactor NHE-RF1	gil 219522018	−0.77	5	24.7	chloride channel regulator activity
UPF0436 protein C9orf6 homologue	gil 194033862	−0.77	2	18	glycine catabolic process
EPLIN-b	gil86450155	−0.77	5	13.2	actin monomers and filaments binding
IGF-binding protein-2	gil1491785	−0.78	3	19.3	regulation of cell growth
hepatoma-derived growth factor-like	gil 335286747	−0.79	5	30	heparin-binding protein
Stathmin	gil75043336	−0.79	2	14.1	regulation of microtubule polymerization or depolymerization
thyroid hormone receptor-associated protein 3	gil 417515856	−0.82	7	9.9	pre-mRNA splicing
phosphatidylethanolamine-binding protein 1-like	gil 311270662	−0.83	4	31	ATP, opioids, and phosphatidylethanolamine binding
A-kinase anchor protein 12	gil 350578047	−0.86	11	14.1	protein kinase A binding
protein DEK	gil 335291759	−0.87	6	22.7	chromatin organization
protein PRRC2C	gil 350588987	−0.87	5	3.1	unknown
APMCF1	gil46241305	−0.89	3	16.9	component of the SRP (signal recognition particle) receptor
LOW QUALITY PROTEIN: protein TFG	gil 350592016	−0.90	3	16.5	signal transducer activity
glia maturation factor beta-like, partial	gil 350579102	−0.91	2	24.1	growth factor activity
hypothetical protein LOC100521629 isoform 1	gil 350585748	−0.92	4	5	mRNA processing
Golgi membrane protein 1-like	gil 350589440	−0.92	2	8.4	unknown
absent in melanoma 1 protein	gil 350578316	−0.92	6	5.5	suppressor of malignant melanoma

dx.doi.org/10.1021/pr500173p | J. Proteome Res. 2014, 13, 5376−5390

Table 1. continued

protein name	accession no.	$\log_2$ ratios (infection/control)	peptides	sequence coverage (%)	functions
proteins present in decreased abundance in TGEV-infected cells					
RNA-binding protein EWS	gil 356461003	−0.93	4	8.3	regulation of transcription
enhancer of rudimentary homologue	gil 297632416	−0.93	2	26.9	cell cycle process
ladinin-1-like	gil 335296241	−0.94	4	13.5	structural molecule activity
translocation protein SEC62	gil 158635942	−0.94	1	6	protein transporter activity
neurogenic locus notch-like protein 2	gil 417515726	−0.95	1	0.6	regulation of cell-fate determination
granulin	gil55247589	−0.95	7	15.8	positive regulation of epithelial cell proliferation
forkhead box protein K2-like	gil 335297203	−0.96	1	2.6	transcription factor activity
actin-related protein 2/3 complex subunit 5	gil 197251940	−0.96	2	23.8	actin binding
huntingtin-interacting protein K-like	gil 311244862	−0.99	2	24.2	chaperone-like activity
membrane-associated progesterone receptor component 1	gil47522662	−1.01	3	20.1	receptor for progesterone
zinc finger CCCH-type containing 18	gil 456753114	−1.01	5	9.4	zinc ion binding
eukaryotic translation initiation factor 3 subunit J-like isoform 1	gil 350578717	−1.04	4	17	translation initiation factor activity
zinc finger protein 768	gil 335284365	−1.05	2	5.2	DNA-dependent RNA polymerase
ferritin L subunit	gil10304378	−1.06	5	40	iron ion binding
60S ribosomal export protein NMD3-like	gil 350591690	−1.08	1	3.4	protein transport
nuclear autoantigenic sperm protein, partial	gil 335309827	−1.09	7	12.4	DNA replication
nuclease-sensitive element-binding protein 1-like	gil 350586335	−1.10	3	14.5	regulation of transcription
regulator of chromosome condensation isoform 2	gil 350585800	−1.12	1	3.1	ran guanyl-nucleotide exchange factor activity
inositol monophosphatase 1	gil68568737	−1.15	4	17	phosphatidylinositol biosynthetic process
brain acid soluble protein 1-like isoform 2	gil 350594172	−1.21	4	33.3	regulation of transcription
tubulin-specific chaperone A-like	gil 350580865	−1.26	1	8.7	tubulin-folding protein
nuclear ubiquitous casein and cyclin-dependent kinases substrate	gil 346644828	−1.28	3	26.7	kinase activity
hypothetical protein LOC100516425	gil 350581286	−1.36	6	9.9	transporter activity
D-tyrosyl-tRNA(Tyr) deacylase 1-like	gil 350594682	−1.38	1	7.2	D-amino acid catabolic process
tyrosine-protein phosphatase nonreceptor type 12	gil 417515862	−1.39	1	1.9	protein tyrosine phosphatase activity
calpastatin	gil 160425377	−1.40	8	13.9	specific inhibition of calpain
hypothetical protein LOC100521745	gil 350590018	−1.64	1	1.3	UBA-like protein

[a]More information is available in Supplementary Table 2, and MS/MS assignment data for single-peptide assignments are provided in Supplementary Data 1.

LC−MS/MS. Of these, 60 proteins were significantly upregulated and 102 proteins were markedly downregulated, based on $\log_2$ ratio of $\geq$0.585 or $\leq$−0.585 and statistically significant differences at $p < 0.05$ (Table 1). Among 162 significantly altered proteins, 24 protein assignments were based on single-peptide assignments. For these proteins, the annotated tandem mass spectra and relevant detailed information were exported by Scaffold software and provided as Supplementary Data 1. The reliability of the results was assessed by labeling and mixing two biological replicates among the control or TGEV-infected samples for proteomic analysis. The difference was plotted versus the percentage of the proteins identified, and it was shown that the proteomic result was of great credibility (Supplementary Figure 1).

Subcellular and Functional Characterization, Biological Processes, and Network Analysis of the Differentially Regulated Proteins

To extend the molecular characterization of these differentially regulated proteins, the Gene Ontology and Uniport databases

dx.doi.org/10.1021/pr500173p | J. Proteome Res. 2014, 13, 5376−5390

were searched to provide relevant information about their biological processes, molecular functions, and cellular components (Supplementary Table 2). We first analyzed the possible subcellular localizations of the 162 identified proteins. As shown in Figure 2A, the 60 proteins upregulated in the TGEV-

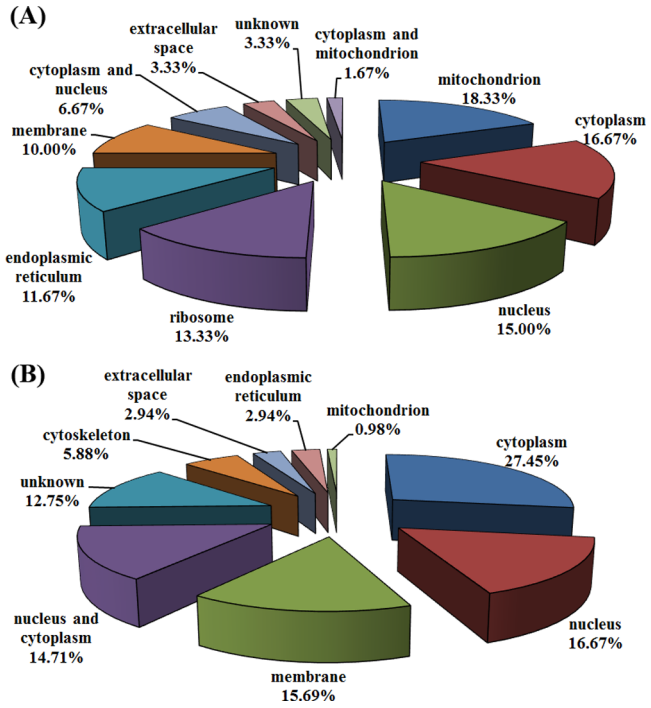

Figure 2. Subcellular annotation of the differentially expressed proteins in PK-15 cells infected with TGEV. (A) Upregulated proteins and (B) downregulated proteins.

infected cells were localized to the mitochondrion (18.33%), cytoplasm (16.67%), nucleus (15.00%), ribosome (13.33%), endoplasmic reticulum (11.67%), membrane (10.00%), nucleus and cytoplasm (6.67%), extracellular space (3.33%), unknown cellular location (3.33%), and cytoplasm and mitochondrion (1.67%). The 102 downregulated proteins were localized to the cytoplasm (27.45%), nucleus (16.67%), membrane (15.69%), nucleus and cytoplasm (14.71%), unknown cellular location (12.75%), cytoskeleton (5.88%), extracellular space (2.94%), endoplasmic reticulum (2.94%), and mitochondrion (0.98%) (Figure 2B).

Because the pig genome database is poorly annotated compared with the human genome, many proteins were unassigned or uncharacterized. Therefore, the gene identifications of the differentially regulated proteins listed in Table 1 were converted to human protein GI numbers. The protein GI numbers and ratios (infection/control) were uploaded into the IPA software, and their functional classification and biological processes analyzed and reconstructed based on the underlying biological evidence from the literature database. According to the functional classification by IPA, these differentially regulated proteins could be divided into four distinctive functional sets: (A) diseases and disorders; (B) molecular and cellular functions; (C) physiological system development and functions; and (D) toxicity functions. These are shown in Figure 3 with their statistical significance ($p < 0.05$), and additional data are given in Supplementary Table 3. These differentially regulated proteins are involved in many biological processes, including infectious diseases, skeletal and muscular disorders, cancer, cellular assembly and organization, and organismal injury and abnormalities.

We also used the IPA tool to explore in detail the potential protein network connections for the differentially regulated proteins. As shown in Figure 4, these differentially regulated proteins could be mapped to nine specific functional networks, and each network had 10 or more "focus" proteins, except network 9 (Supplementary Table 3). The four most strongly represented networks of interest corresponded to (1) cellular development, cellular assembly and organization, and protein synthesis (30 molecules; Figure 5A); (2) cellular assembly and organization, cellular function and maintenance, and cancer (24 molecules; Figure 5B); (3) cell cycle, cellular assembly and organization, and behavior (17 molecules; Figure 5C); and (4) infectious disease, antimicrobial response, and inflammatory response (16 molecules; Figure 5D). Among the differentially expressed proteins represented in the network analysis, the upregulated proteins are shown in shades of red and the downregulated proteins in shades of green. Other proteins in these networks that were not identified in our study are shown in white.

TGEV Infection Induces the Phosphorylation and Nuclear Translocation of STAT1 and Antiviral Gene Expression

To confirm the LC−MS/MS data, four representative proteins (GAPDH, calpastatin, Mx1, and STAT1) were selected for immunoblotting analysis with antibodies specific for these proteins. The proteins were selected on the basis of interest but also on their different ratios. As shown in Figure 6A, the ratios from the immunoblotting analysis identified four representative proteins (GAPDH, calpastatin, Mx1, and STAT1), in agreement with those identified with iTRAQ approaches.

When we analyzed the 60 upregulated proteins individually (Table 1), we found that eight of the 10 most upregulated proteins were encoded by interferon-stimulated genes (ISGs), including ISG15, interferon-induced protein with tetratricopeptide repeats 1 (IFIT1), IFIT2, IFIT3, Mx1, Mx2, 2′-5′-oligoadenylate synthetase 1 (OAS1), and OAS2. STAT1, a critical regulator of the interferon signaling pathway,[25,26] was also significantly upregulated (1.724-$\log_2$-fold, infection vs control) and rated 11th among the most upregulated proteins. The upregulation of Mx1 and STAT1 was confirmed by immunoblotting (Figure 6A). Because no specific antibodies against porcine ISG15, IFIT1−3, Mx2, or OAS1−2 are available, and no cross-reaction could be detected with antibodies against the homologous human proteins (data not shown), real-time RT-PCR was used to analyze the expression of the seven ISGs. To this end, PK-15 cells were mock-infected or infected with TGEV at MOI = 0.1. The cells were collected at 12 and 24 hpi and subjected to real-time RT-PCR using gene-specific primers (Supplementary Table 1). As shown in Figure 6B, the expression of all seven ISGs was significantly upregulated in the TGEV-infected cells in a time-dependent manner, compared with their expression in the mock-infected cells. These results further confirmed the data obtained with the iTRAQ approach.

It is well-known that ISG production is mainly mediated by interferon via the JAK-STAT signaling pathway, which is initiated by binding to the cell-surface interferon receptors, leading to the activation of JAK1 and TYK2 through tyrosine phosphorylation. The phosphorylated JAK−receptor complex recruits and phosphorylates various STAT proteins. The

dx.doi.org/10.1021/pr500173p | J. Proteome Res. 2014, 13, 5376−5390

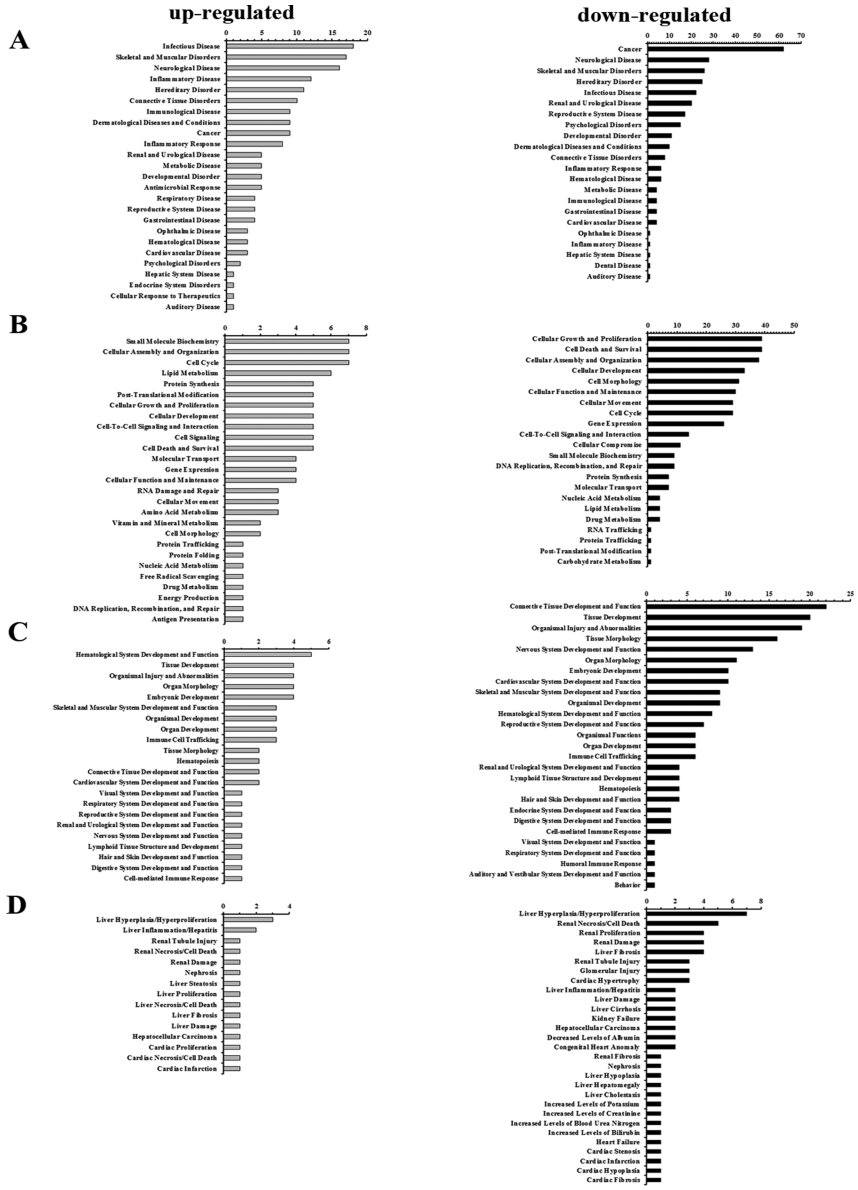

Figure 3. Functional characterization of the upregulated and downregulated proteins. (A) Diseases and disorders, (B) molecular and cellular functions, (C) physiological system development and functions, and (D) toxicity functions. More information is available in Supplementary Table 3.

phosphorylated STATs then form homodimers or heterodimers and translocate into the nucleus to induce the transcription of ISGs.[27,28] Therefore, the phosphorylation and nuclear accumulation of the STAT proteins are two hallmarks of the activation of the classical JAK-STAT pathway. Because STAT1 and many ISGs were significantly upregulated in TGEV-infected cells, the next question is whether TGEV infection induces STAT1 phosphorylation and nuclear accumulation. To test this possibility, PK-15 cells were infected with TGEV at MOI = 0.1 and collected at 24 hpi, and the total and phosphorylated STAT1 was measured. As shown in Figure 7A, phosphorylated STAT1 was dramatically increased in the TGEV-infected cells compared with that in the mock-infected cells. Total STAT1 was also upregulated in the TGEV-infected cells as observed with a quantitative proteomic analysis.

To determine whether TGEV infection promotes STAT1 nuclear translocation, PK-15 cells were untreated or infected with TGEV at MOI = 0.1 for 24 h, after which they were fixed and immunostained with a monoclonal antibody directed against the TGEV N protein and then with Cy3-conjugated goat anti-mouse IgG antibody, rabbit polyclonal antibody directed against STAT1 and then with FITC-labeled goat anti-rabbit IgG, respectively. As shown in Figure 7B, STAT1 remained in the cytoplasm in the mock-infected cells, while obvious nuclear accumulation of STAT1 in TGEV-infected cells. It should be noted that the nuclear translocation of STAT1 could also be observed in some uninfected surrounding cells. It is possible that the released type I IFN from TGEV-infected cells stimulates the uninfected surrounding cells, resulting in nuclear translocation of STAT1.

DISCUSSION

Quantitative proteomic methods are widely accepted tools with which to study virus−host cell interactions. In this study, we used an iTRAQ approach to identify the differentially regulated proteins in PK-15 cells during TGEV infection. In total, we obtained relative quantitative information for 3062 proteins and identified 162 proteins differentially expressed in TGEV-

dx.doi.org/10.1021/pr500173p | J. Proteome Res. 2014, 13, 5376−5390

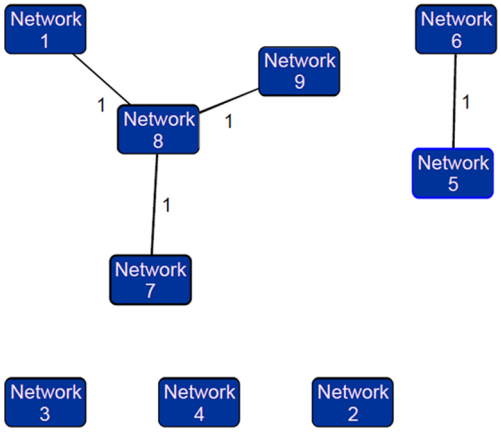

Figure 4. Overview of specific functional networks. Each network contains at least 10 "focus" proteins (significantly up- or down-regulated proteins), except network 9. The numbers between two networks represent the numbers of overlapping proteins. More information is available in Supplementary Table 3.

infected PK-15 cells. By analyzing these differentially expressed proteins in detail, we gained insight into the interaction between TGEV and its host cells, including the cellular response to TGEV infection and the cellular mechanisms involved in viral pathogenesis.

One of the major findings of the proteomic analysis in our study was that TGEV infection induces JAK-STAT signaling. As early as in 1981, La Bonnardiere and Laude first detected high levels of both local and systemic type I interferon activity in TGEV-infected piglets.[29] Charley and Laude also detected high levels of interferon synthesis in the culture fluids of TGEV-infected cells incubated with porcine peripheral blood mononuclear cells.[30] In a subsequent study, the infection of neonatal pigs with a virulent strain of TGEV caused a significant increase in serum interferon and enterocyte 2′-5′-OAS activity compared with that in the control pigs.[31] These early observations support the view that TGEV infection induces interferon production in vitro and in vivo. Although Baudoux et al. found that the coexpression of TGEV M and E proteins induced an interferogenic activity similar to that of the

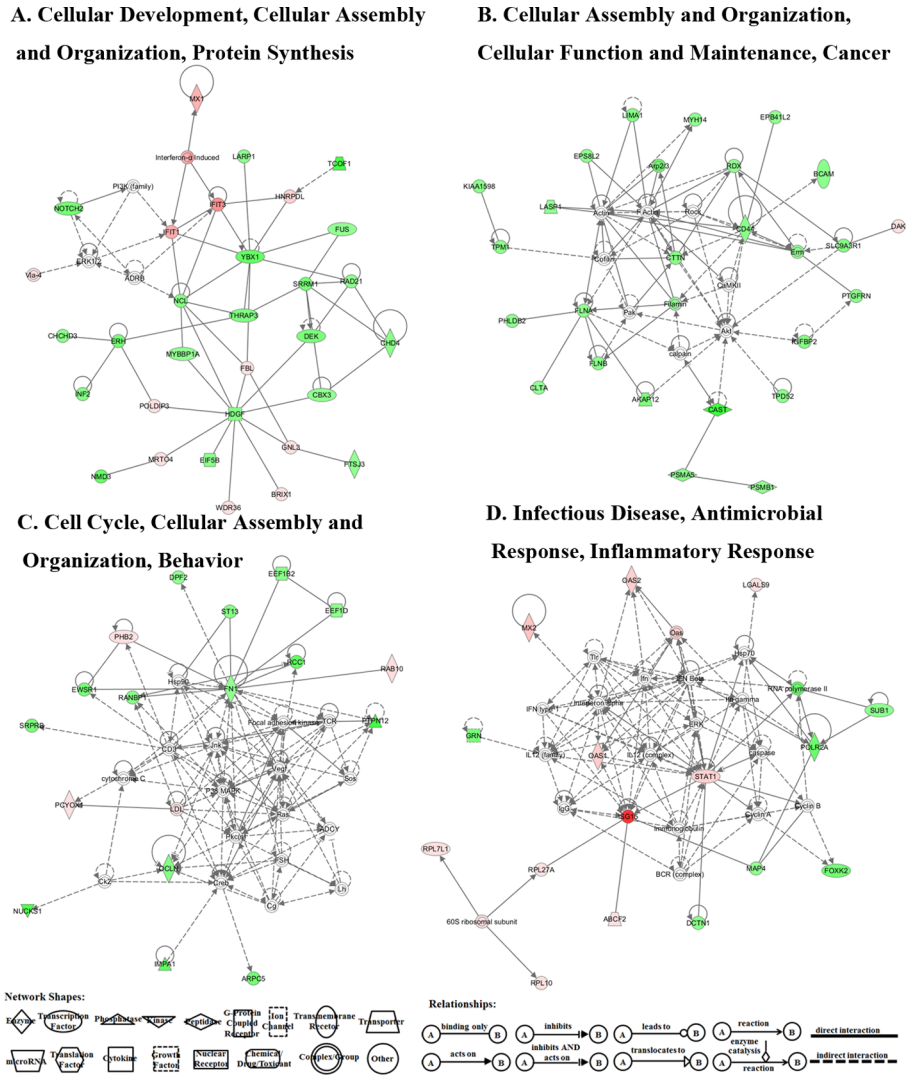

Figure 5. Specific network analysis of proteins significantly altered in TGEV-infected cells using the IPA tool. Significantly upregulated proteins are shown in red; significantly downregulated proteins are in green; and proteins that were not identified in this study but are involved in the networks are shown in white. The color depth indicates the magnitude of the change in protein expression. The shapes are indicative of the molecular class, and the lines with arrows indicate the molecular relationships.

dx.doi.org/10.1021/pr500173p | J. Proteome Res. 2014, 13, 5376−5390

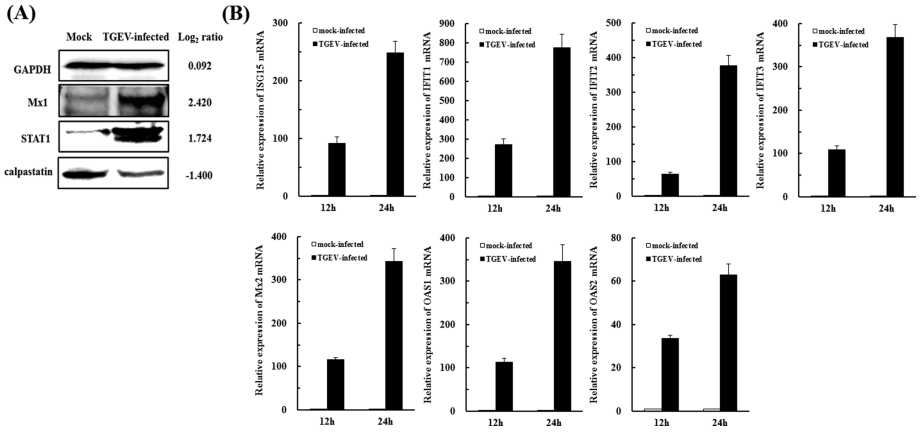

Figure 6. Confirmation of differentially expressed proteins with immunoblotting analysis or real-time RT-PCR. (A) Immunoblotting analysis of GAPDH, STAT1, Mx1, and calpastatin in TGEV-infected and control samples. iTRAQ ratios (infection/control) are shown on the right side. (B) Real-time RT-PCR analysis of the upregulated expression of ISGs in TGEV-infected cells and controls. PK-15 cells were infected with TGEV or mock-infected at MOI = 0.1. The cells were collected at 12 and 24 hpi for real-time RT-PCR to analyze the relative expression of ISG15, IFIT1, IFIT2, IFIT3, OAS1, OAS2, and Mx2 mRNAs.

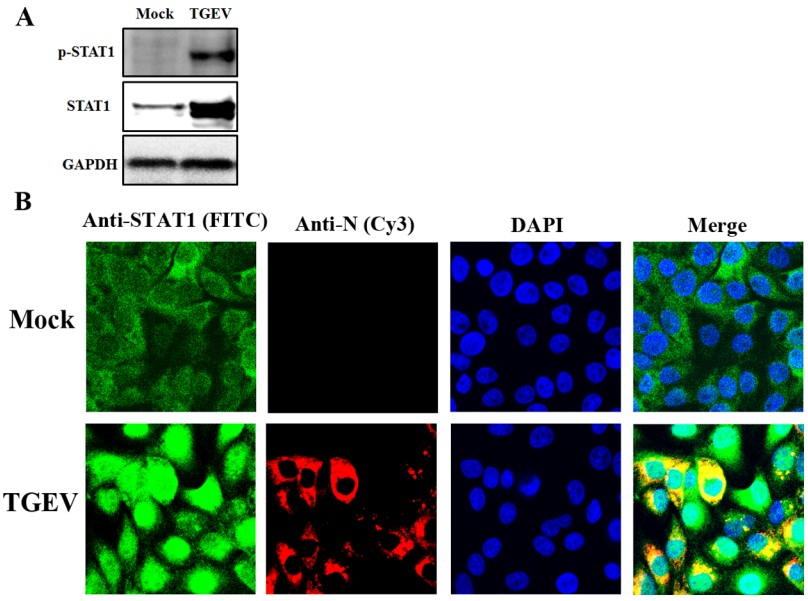

Figure 7. TGEV infection induced the phosphorylation and nuclear translocation of STAT1. (A) TGEV infection enhanced the phosphorylation of STAT1. PK-15 cells were infected with TGEV at MOI = 0.1 or mock-infected. Cells were collected at 24 hpi for immunoblotting to detect the protein levels of total STAT1 and phosphorylated STAT1. (B) TGEV infection induced the nuclear translocation of STAT1. PK-15 cells were infected with TGEV at MOI = 0.1 or mock-infected. At 24 hpi, cells were fixed with cold 4% paraformaldehyde, subjected to immunofluorescence staining with antibodies against TGEV N protein and STAT1, respectively. Cell nuclei were counterstained with 0.01% 4′,6-diamidino-2-phenylindole (DAPI). The fluorescent images were examined under a confocal laser scanning microscope (LSM 510 Meta, Carl Zeiss).

complete virions,[32] the molecular mechanism, especially the signaling pathway used by TGEV to induce interferon, remained largely unknown. In the present study, eight ISGs, encoding some important antiviral proteins, such as ISG15, Mx1, Mx2, OAS1, and OAS2, were shown with quantitative proteomics to be upregulated in TGEV-infected cells. The differential expression of these proteins was confirmed with immunoblotting or real-time RT-PCR. These results support the previous view that TGEV infection induces the over-expression of many antiviral proteins. In this study, we also confirmed with proteomics and immunoblotting that STAT1, a key regulator of the interferon-responsive genes, was upregulated during TGEV infection. TGEV infection also enhanced the phosphorylation and nuclear translocation of STAT1, suggesting that TGEV activates canonical interferon signaling through the JAK-STAT1 pathway.

In this study, LC−MS/MS identified armadillo repeat containing 10 (ARMC10) as a protein upregulated by TGEV infection. ARMC10 is a major structural component of importin α, which consists of 10 tandemly repeated armadillo repeats (ARM), each formed by three α-helices.[33] Some viral proteins, such as HIV-1 integrase and DENV-2 NS5,[34,35] can utilize the importin α/β superfamily of transport proteins for efficient virus production, and this process can be blocked by ivermectin, a potential inhibitor of importin α/β-mediated transport.[36] We speculated that, during TGEV infection, an increase in ARMC10 would support the transport of TGEV proteins, promoting its propagation. Nardozzi et al. showed that the nuclear transport of tyrosine-phosphorylated STAT1

dx.doi.org/10.1021/pr500173p | J. Proteome Res. 2014, 13, 5376−5390

relies on its specific and high-affinity binding to the importin α5 C-terminal acidic tail, in which ARM repeat 10 is located.[37] Recent research has shown that PRRSV Nsp1β and hepatitis B virus polymerase (two viruses known to inhibit interferon production) impair interferon-activated JAK-STAT signal transduction by inducing the degradation and inhibition of importin α5 (also called karyopherin-α1), respectively.[38,39] The relationship between the upregulation of ARM repeat 10 and the activation of the JAK-STAT1 signaling pathway in TGEV-infected cells is an interesting issue and is being investigated in our laboratory.

TGEV is a porcine enteropathogenic coronavirus that causes lethal watery diarrhea and severe dehydration in piglets. The intestinal and renal proximal tubule brush border Na^+/H^+ exchanger NHE3, which is the most important sodium absorptive transporter and is responsible for the majority of electroneutral salt absorption in the intestine, binds to members of the Na^+/H^+ exchanger regulatory factor (NHERF) family. They are present in locations in or close to the brush border and scaffold a variable series of proteins in NHE3-containing complexes in a dynamic manner, and this binding is altered by changes in signal transduction, which affect NHE3 activity.[40] NHERF1 plays a critical role in establishing and maintaining the integrity of the intestinal barrier function and was significantly downregulated in this study, as shown in Table 1. Some previous studies have suggested that, in addition to reducing Na^+ absorption by regulating NHE3, NHERF1 downregulation results in increased intestinal epithelial permeability, a recognized mechanism of microbe-mediated pathogenesis in inflammatory bowel disease (IBD).[41,42] One of the mechanisms that most frequently contribute to diarrhea in TGEV-infected piglets is altered intestinal sodium transport, with the accumulation of electrolytes and water in the intestinal lumen. Butler et al. studied 3 week old piglets 40 h after experimental infection with TGEV to identify the mechanism of diarrhea and found that disordered sodium transport played an important role in the pathogenesis of this disease.[43] We speculated that the downregulation of NHERF1 by TGEV causes the inactivation of the sodium pump in the intestinal epithelial cells, which leads in turn to diarrhea in the piglets by increasing the osmotic pressure. The inflammation-induced downregulation of PDZK1 (a member of the NHERF family) may contribute to the pathogenesis of inflammatory diarrhea in IBD.[44] Therefore, the dysregulation of salt and water transport by NHE3 dysfunction may be mediated by the TGEV-induced inflammatory response. Overall, our study provides new insight into the pathogenesis of diarrhea in TGEV-infected piglets.

Cytoskeletal changes are associated with transcellular membrane trafficking, which is necessary for viral replication. Changes in several key microfilament-associated and microtubule-associated proteins, such as actin and tubulin, have been detected in SARS-CoV and infectious bursal disease virus (IBDV) infection.[16,45] Most of the cytoskeletal changes detected in TGEV-infected cells were downregulated in this study (Table 1), which is similar to the results of proteomic studies of IBDV and PCV2.[18,45] Among these proteins, filamin-A and filamin-B are actin-binding and signal mediator scaffolding proteins that cross-link actin filaments and link actin filaments to membrane glycoproteins. Microtubule-associated protein 4 is a member of a heterogeneous group of proteins that have microtubule-binding domains, which stabilize microtubules.[46] Actin-related protein 2/3 complex subunit 5 plays an important role in regulating the rear polarization of the microtubule-organizing center by organizing the actin and microtubule cytoskeletons in neointimal smooth muscle cells.[47] In this study, these proteins, related to the organization of the actin cytoskeleton, showed relatively reduced expression after TGEV infection. We speculated that, in the host cell, the actin cytoskeleton network collapses and disperses, leading to an unstable cytoskeletal structure. This cytoskeletal disruption may facilitate the release of TGEV particle from the infected cells. Interestingly, the activity of NHE3 may be dependent upon the stabilization of the cytoskeletal proteins that adhere to NHERF1,[48] so TGEV-induced cytoskeletal disruption may also cause the functional disturbance of water and sodium transport.

When we were preparing this article, a paper was published by Zhang and colleagues in which they used a 2D difference gel electrophoresis (DIGE)-based proteomic approach to survey TGEV-infected ST cells and identified 33 differentially expressed host proteins. However, they found no immune-response-related proteins in the TGEV-infected ST cells and speculated that this was attributable to the host cells chosen or the fact that an attenuated TGEV strain was used.[49] Strain WH-1, used in our present study, is a virulent TGEV, and we used an iTRAQ approach to identify the differentially expressed cellular proteins in PK-15 cells during TGEV infection. iTRAQ is a highly sensitive technique that allows the simultaneous quantitation of proteins in multiple samples when combined with multidimensional LC−MS/MS analysis and has drawn increasing interest and application in proteomic research. A comparative study of three quantitative proteomic methods showed that the global-tagging iTRAQ technique is more sensitive than the cysteine-specific cICAT method or the DIGE technique.[50] Although iTRAQ has many significant advantages over other traditional proteomic approaches, the nucleocapsid protein was the only viral protein identified in this study (Supplementary Table 4). It is well-known that the nucleocapsid protein is most abundantly expressed during the replication cycle of TGEV.[51] Over 100 ISGs are encoded by host cells, but the expression of only eight ISGs was identified as upregulated in the present study. Here, we speculated that these differentially expressed proteins identified in our study should be highly abundant in the samples and probably missed many other antiviral proteins. Therefore, it was imperative that a new technique be developed for quantitative proteomic analysis to provide more comprehensive data.

In summary, the proteomic changes in TGEV-infected PK-15 cells were characterized using iTRAQ coupled to LC−MS/MS. A comprehensive pathogen−host protein interaction network in TGEV-infected PK-15 cells was identified in this study. Although many significantly up- or downregulated proteins and pathways are closely related to the symptoms of or pathological responses to TGEV infection, further functional investigations are required to understand the pathogenic mechanisms and molecular responses of host cells to TGEV infection. Further research may identify therapeutic targets or lead to the development of new methods for preventing TGEV infection.

■ ASSOCIATED CONTENT

Supporting Information

Supplementary Table 1: The sequences of primers used in this study for real-time RT-PCR. Supplementary Table 2: Information for each significantly altered protein ($p < 0.05$)

dx.doi.org/10.1021/pr500173p | J. Proteome Res. 2014, 13, 5376−5390

identified in TGEV-infected cells, and GO analysis. Supplementary Table 3: Information for GI transfer, functional characterization of up- and downregulated proteins in TGEV-infected cells, Network analysis of the differentially regulated proteins. Supplementary Table 4: Viral proteins identified in TGEV-infected cells. Supplementary Figure 1: Repeatability between biological replicates of iTRAQ LC−MS/MS proteomic analysis. Supplementary Data 1: The annotated tandem mass spectra and the detailed information regarding protein assignments based on single-peptide assignments. This material is available free of charge via the Internet at http://pubs.acs.org.

AUTHOR INFORMATION

Corresponding Authors

*Tel: +86 27 8728 6884. Fax: +86 27 8728 2608. E-mail: fanglr@mail.hzau.edu.cn (L.F.).
*Tel: +86 27 8728 6884. Fax: +86 27 8728 2608. E-mail: vet@mail.hzau.edu.cn (S.X.).

Notes

The authors declare no competing financial interest.

ACKNOWLEDGMENTS

This work was supported by the National Natural Sciences Foundation of China (31225027, 31402181, 31121004) and the Fundamental Research Funds for the Central Universities (2013PY043).

REFERENCES

(1) Garwes, D. J. Transmissible gastroenteritis. *Vet. Rec* **1988**, *122* (19), 462−3.
(2) Mullan, B. P.; Davies, G. T.; Cutler, R. S. Simulation of the economic impact of transmissible gastroenteritis on commercial pig production in Australia. *Aust. Vet. J.* **1994**, *71* (5), 151−4.
(3) Laude, H.; Rasschaert, D.; Delmas, B.; Godet, M.; Gelfi, J.; Charley, B. Molecular biology of transmissible gastroenteritis virus. *Vet. Microbiol.* **1990**, *23* (1−4), 147−54.
(4) Eleouet, J. F.; Rasschaert, D.; Lambert, P.; Levy, L.; Vende, P.; Laude, H. Complete sequence (20 kilobases) of the polyprotein-encoding gene 1 of transmissible gastroenteritis virus. *Virology* **1995**, *206* (2), 817−22.
(5) Putics, A.; Gorbalenya, A. E.; Ziebuhr, J. Identification of protease and ADP-ribose 1″-monophosphatase activities associated with transmissible gastroenteritis virus non-structural protein 3. *J. Gen. Virol.* **2006**, *87* (Pt 3), 651−6.
(6) Yount, B.; Curtis, K. M.; Baric, R. S. Strategy for systematic assembly of large RNA and DNA genomes: transmissible gastroenteritis virus model. *J. Virol.* **2000**, *74* (22), 10600−11.
(7) Schwegmann-Wessels, C.; Zimmer, G.; Laude, H.; Enjuanes, L.; Herrler, G. Binding of transmissible gastroenteritis coronavirus to cell surface sialoglycoproteins. *J. Virol.* **2002**, *76* (12), 6037−43.
(8) Escors, D.; Camafeita, E.; Ortego, J.; Laude, H.; Enjuanes, L. Organization of two transmissible gastroenteritis coronavirus membrane protein topologies within the virion and core. *J. Virol.* **2001**, *75* (24), 12228−40.
(9) Escors, D.; Ortego, J.; Laude, H.; Enjuanes, L. The membrane M protein carboxy terminus binds to transmissible gastroenteritis coronavirus core and contributes to core stability. *J. Virol.* **2001**, *75* (3), 1312−24.
(10) Maeda, J.; Repass, J. F.; Maeda, A.; Makino, S. Membrane topology of coronavirus E protein. *Virology* **2001**, *281* (2), 163−9.
(11) Ortego, J.; Ceriani, J. E.; Patino, C.; Plana, J.; Enjuanes, L. Absence of E protein arrests transmissible gastroenteritis coronavirus maturation in the secretory pathway. *Virology* **2007**, *368* (2), 296−308.
(12) Sola, I.; Alonso, S.; Zuniga, S.; Balasch, M.; Plana-Duran, J.; Enjuanes, L. Engineering the transmissible gastroenteritis virus genome as an expression vector inducing lactogenic immunity. *J. Virol.* **2003**, *77* (7), 4357−69.
(13) Ortego, J.; Sola, I.; Almazan, F.; Ceriani, J. E.; Riquelme, C.; Balasch, M.; Plana, J.; Enjuanes, L. Transmissible gastroenteritis coronavirus gene 7 is not essential but influences in vivo virus replication and virulence. *Virology* **2003**, *308* (1), 13−22.
(14) Emmott, E.; Rodgers, M. A.; Macdonald, A.; McCrory, S.; Ajuh, P.; Hiscox, J. A. Quantitative proteomics using stable isotope labeling with amino acids in cell culture reveals changes in the cytoplasmic, nuclear, and nucleolar proteomes in Vero cells infected with the coronavirus infectious bronchitis virus. *Mol. Cell. Proteomics* **2010**, *9* (9), 1920−36.
(15) Zhang, L. K.; Chai, F.; Li, H. Y.; Xiao, G.; Guo, L. Identification of host proteins involved in Japanese encephalitis virus infection by quantitative proteomics analysis. *J. Proteome Res.* **2013**, *12* (6), 2666−78.
(16) Jiang, X. S.; Tang, L. Y.; Dai, J.; Zhou, H.; Li, S. J.; Xia, Q. C.; Wu, J. R.; Zeng, R. Quantitative analysis of severe acute respiratory syndrome (SARS)-associated coronavirus-infected cells using proteomic approaches: implications for cellular responses to virus infection. *Mol. Cell. Proteomics* **2005**, *4* (7), 902−13.
(17) Coombs, K. M.; Berard, A.; Xu, W.; Krokhin, O.; Meng, X.; Cortens, J. P.; Kobasa, D.; Wilkins, J.; Brown, E. G. Quantitative proteomic analyses of influenza virus-infected cultured human lung cells. *J. Virol.* **2010**, *84* (20), 10888−906.
(18) Fan, H.; Ye, Y.; Luo, Y.; Tong, T.; Yan, G.; Liao, M. Quantitative proteomics using stable isotope labeling with amino acids in cell culture reveals protein and pathway regulation in porcine circovirus type 2 infected PK-15 cells. *J. Proteome Res.* **2012**, *11* (2), 995−1008.
(19) Huang, X.; Stone, D. K.; Yu, F.; Zeng, Y.; Gendelman, H. E. Functional proteomic analysis for regulatory T cell surveillance of the HIV-1-infected macrophage. *J. Proteome Res.* **2010**, *9* (12), 6759−73.
(20) Zhang, J.; Niu, D.; Sui, J.; Ching, C. B.; Chen, W. N. Protein profile in hepatitis B virus replicating rat primary hepatocytes and HepG2 cells by iTRAQ-coupled 2-D LC−MS/MS analysis: insights on liver angiogenesis. *Proteomics* **2009**, *9* (10), 2836−45.
(21) Feng, X.; Zhang, J.; Chen, W. N.; Ching, C. B. Proteome profiling of Epstein-Barr virus infected nasopharyngeal carcinoma cell line: identification of potential biomarkers by comparative iTRAQ-coupled 2D LC/MS-MS analysis. *J. Proteomics* **2011**, *74* (4), 567−76.
(22) Lu, Q.; Bai, J.; Zhang, L.; Liu, J.; Jiang, Z.; Michal, J. J.; He, Q.; Jiang, P. Two-dimensional liquid chromatography-tandem mass spectrometry coupled with isobaric tags for relative and absolute quantification (iTRAQ) labeling approach revealed first proteome profiles of pulmonary alveolar macrophages infected with porcine reproductive and respiratory syndrome virus. *J. Proteome Res.* **2012**, *11* (5), 2890−903.
(23) Liu, J.; Bai, J.; Lu, Q.; Zhang, L.; Jiang, Z.; Michal, J. J.; He, Q.; Jiang, P. Two-dimensional liquid chromatography-tandem mass spectrometry coupled with isobaric tags for relative and absolute quantification (iTRAQ) labeling approach revealed first proteome profiles of pulmonary alveolar macrophages infected with porcine circovirus type 2. *J. Proteomics* **2013**, *79*, 72−86.
(24) Bradford, M. M. A rapid and sensitive method for the quantitation of microgram quantities of protein utilizing the principle of protein-dye binding. *Anal. Biochem.* **1976**, *72*, 248−54.
(25) Darnell, J. E., Jr.; Kerr, I. M.; Stark, G. R. JAK-STAT pathways and transcriptional activation in response to IFNs and other extracellular signaling proteins. *Science* **1994**, *264* (5164), 1415−21.
(26) Platanias, L. C. Mechanisms of type-I- and type-II-interferon-mediated signalling. *Nat. Rev. Immunol.* **2005**, *5* (5), 375−86.
(27) Darnell, J. E., Jr. STATs and gene regulation. *Science* **1997**, *277* (5332), 1630−5.
(28) Shuai, K.; Liu, B. Regulation of JAK-STAT signalling in the immune system. *Nat. Rev. Immunol.* **2003**, *3* (11), 900−11.
(29) La Bonnardiere, C.; Laude, H. High interferon titer in newborn pig intestine during experimentally induced viral enteritis. *Infect. Immun.* **1981**, *32* (1), 28−31.

(30) Charley, B.; Laude, H. Induction of alpha interferon by transmissible gastroenteritis coronavirus: role of transmembrane glycoprotein E1. *J. Virol.* **1988**, *62* (1), 8−11.
(31) Bosworth, B. T.; MacLachlan, N. J.; Johnston, M. I. Induction of the 2-5A system by interferon and transmissible gastroenteritis virus. *J. Interferon Res.* **1989**, *9* (6), 731−9.
(32) Baudoux, P.; Carrat, C.; Besnardeau, L.; Charley, B.; Laude, H. Coronavirus pseudoparticles formed with recombinant M and E proteins induce alpha interferon synthesis by leukocytes. *J. Virol.* **1998**, *72* (11), 8636−43.
(33) Nardozzi, J. D.; Lott, K.; Cingolani, G. Phosphorylation meets nuclear import: a review. *Cell Commun. Signaling* **2010**, *8*, 32.
(34) Hearps, A. C.; Jans, D. A. HIV-1 integrase is capable of targeting DNA to the nucleus via an importin alpha/beta-dependent mechanism. *Biochem. J.* **2006**, *398* (3), 475−84.
(35) Pryor, M. J.; Rawlinson, S. M.; Butcher, R. E.; Barton, C. L.; Waterhouse, T. A.; Vasudevan, S. G.; Bardin, P. G.; Wright, P. J.; Jans, D. A.; Davidson, A. D. Nuclear localization of dengue virus nonstructural protein 5 through its importin alpha/beta-recognized nuclear localization sequences is integral to viral infection. *Traffic* **2007**, *8* (7), 795−807.
(36) Wagstaff, K. M.; Sivakumaran, H.; Heaton, S. M.; Harrich, D.; Jans, D. A. Ivermectin is a specific inhibitor of importin alpha/beta-mediated nuclear import able to inhibit replication of HIV-1 and dengue virus. *Biochem. J.* **2012**, *443* (3), 851−6.
(37) Nardozzi, J.; Wenta, N.; Yasuhara, N.; Vinkemeier, U.; Cingolani, G. Molecular basis for the recognition of phosphorylated STAT1 by importin alpha5. *J. Mol. Biol.* **2010**, *402* (1), 83−100.
(38) Wang, R.; Nan, Y.; Yu, Y.; Zhang, Y. J. Porcine reproductive and respiratory syndrome virus Nsp1beta inhibits interferon-activated JAK/STAT signal transduction by inducing karyopherin-alpha1 degradation. *J. Virol.* **2013**, *87* (9), 5219−28.
(39) Chen, J.; Wu, M.; Zhang, X.; Zhang, W.; Zhang, Z.; Chen, L.; He, J.; Zheng, Y.; Chen, C.; Wang, F.; Hu, Y.; Zhou, X.; Wang, C.; Xu, Y.; Lu, M.; Yuan, Z. Hepatitis B virus polymerase impairs interferon-alpha-induced STA T activation through inhibition of importin-alpha5 and protein kinase C-delta. *Hepatology* **2013**, *57* (2), 470−82.
(40) Donowitz, M.; Cha, B.; Zachos, N. C.; Brett, C. L.; Sharma, A.; Tse, C. M.; Li, X. NHERF family and NHE3 regulation. *J. Physiol.* **2005**, *567* (Pt 1), 3−11.
(41) Sartor, R. B. Mechanisms of disease: pathogenesis of Crohn's disease and ulcerative colitis. *Nat. Clin. Pract. Gastroenterol. Hepatol.* **2006**, *3* (7), 390−407.
(42) Strober, W.; Fuss, I.; Mannon, P. The fundamental basis of inflammatory bowel disease. *J. Clin. Invest.* **2007**, *117* (3), 514−21.
(43) Butler, D. G.; Gall, D. G.; Kelly, M. H.; Hamilton, J. R. Transmissible gastroenteritis. Mechanisms responsible for diarrhea in an acute viral enteritis in piglets. *J. Clin. Invest.* **1974**, *53* (5), 1335−42.
(44) Lenzen, H.; Lunnemann, M.; Bleich, A.; Manns, M. P.; Seidler, U.; Jorns, A. Downregulation of the NHE3-binding PDZ-adaptor protein PDZK1 expression during cytokine-induced inflammation in interleukin-10-deficient mice. *PLoS One* **2012**, *7* (7), e40657.
(45) Zheng, X.; Hong, L.; Shi, L.; Guo, J.; Sun, Z.; Zhou, J. Proteomics analysis of host cells infected with infectious bursal disease virus. *Mol. Cell. Proteomics* **2008**, *7* (3), 612−25.
(46) Olmsted, J. B. Microtubule-associated proteins. *Annu. Rev. Cell Biol.* **1986**, *2*, 421−57.
(47) Silverman-Gavrila, R.; Silverman-Gavrila, L.; Hou, G.; Zhang, M.; Charlton, M.; Bendeck, M. P. Rear polarization of the microtubule-organizing center in neointimal smooth muscle cells depends on PKCalpha, ARPC5, and RHAMM. *Am. J. Pathol.* **2011**, *178* (2), 895−910.
(48) Kurashima, K.; D'Souza, S.; Szaszi, K.; Ramjeesingh, R.; Orlowski, J.; Grinstein, S. The apical Na(+)/H(+) exchanger isoform NHE3 is regulated by the actin cytoskeleton. *J. Biol. Chem.* **1999**, *274* (42), 29843−9.
(49) Zhang, X.; Shi, H. Y.; Chen, J. F.; Shi, D.; Lang, H. W.; Wang, Z. T.; Feng, L. Identification of cellular proteome using two-dimensional difference gel electrophoresis in ST cells infected with transmissible gastroenteritis coronavirus. *Proteome Sci.* **2013**, *11* (1), 31.
(50) Wu, W. W.; Wang, G.; Baek, S. J.; Shen, R. F. Comparative study of three proteomic quantitative methods, DIGE, cICAT, and iTRAQ, using 2D gel- or LC-MALDI TOF/TOF. *J. Proteome Res.* **2006**, *5* (3), 651−8.
(51) Hiscox, J. A.; Cavanagh, D.; Britton, P. Quantification of individual subgenomic mRNA species during replication of the coronavirus transmissible gastroenteritis virus. *Virus Res.* **1995**, *36* (2−3), 119−30.